Chinese Chemical Letters 36 (2025) 109669

Contents lists available at ScienceDirect

Chinese Chemical Letters

journal homepage: www.elsevier.com/locate/cclet

Growth of CeCo-MOF in dendritic mesoporous organosilica as highly efficient antioxidant for enhanced thermal stability of silicone rubber

Guizhi Zhu[a,b], Junrui Tan[a], Longfei Tan[a,*], Qiong Wu[a], Xiangling Ren[a], Changhui Fu[a], Zhihui Chen[b,*], Xianwei Meng[a,*]

[a] State Key Laboratory of Cryogenic Science and Technology, Technical Institute of Physics and Chemistry, Chinese Academy of Sciences, Beijing 100190, China
[b] School of Materials Science and Engineering, Changzhou University, Changzhou 213164, China

ARTICLE INFO

Article history:
Received 25 December 2023
Revised 20 February 2024
Accepted 22 February 2024
Available online 23 February 2024

Keywords:
Mesoporous organosilica nanoparticles
Silicone rubber
Metal-organic framework
Antioxidants
Thermal stability
Thermal oxidative degradation

ABSTRACT

High-efficient rubber antioxidants for enhanced heat resistance without compromising mechanical properties remain an enormous and long-term challenge for the rubber industry. Herein, we employed the *in-situ* growth of Ce-doped Co-metal-organic framework (CeCo-MOF) in dendritic mesoporous organosilica nanoparticles (DMONs@CeCo-MOF, denoted as DCCM) to prepare a novel antioxidant that exhibit outstanding thermal stability. Dendritic mesoporous organosilica nanoparticles (DMONs) effectively alleviated the incompatibility of CeCo-MOF in the polymer matrix, and the effective scavenging of free radicals was attributed to the various oxidation states of metal ions in CeCo-MOF. Surprising, by adding only 0.5 phr (parts per hundred of rubber) of DMONs@CeCo-MOF to silicone rubber, (SR), the retention rate of tensile strength increased from 37.3% to 61.6% after aging 72 h at 250 °C, and the retention rate of elongation at break of DCCM/SR1 composites reached 68%, which was 5.43 times of SR. The strategy of anchoring MOFs on the surface of silica also provides a viable method for preparing effective compound functionalized rubber antioxidant.

Silicone rubber (SR) shows promise for aerospace and automotive manufacturing since they possess outstanding mechanical property, wide range of operating temperatures, as well as chemical stability [1]. However, the longevity of rubber products fluctuates based on the conditions and duration of operation, such as heat, oxygen, lighting, and other chemicals [2–4]. These factors can result in the premature aging of rubber products and unstable mechanical properties, and ultimately destroy their duration as either raw materials or finished products. Thermal-oxidative aging is the most common type of rubber aging. Unfortunately, the insufficient antioxidant efficiency of traditional antioxidants, the intrinsic toxicity and blooming/migration issues of antioxidants hinder the development of heat-resistant rubber [5–7]. It has been revealed that the oxidative degradation of polymers is a series of free radical chain reactions that can be inhibited by scavenging free radicals [8]. Therefore, efforts have been thrown on incorporating several heat-resistant fillers into the rubber system or assembling numerous antioxidant groups (phosphates, rare-earth ions, transition metal ion, *etc.*) which could react with free radicals into one structure to obstruct the free radical chain reactions. Nevertheless, the production of most antioxidants, such as amides, phenols, and amines, depends on non-renewable fossil fuels, and low active sites on the surface also limits antioxidant efficiency. Wu *et al.* [9] synthesized a cerium-iron composite oxide *via* a citric acid sol-gel method to be utilized as a heat-resistant additive for SR, and the thermal oxidative stability and mechanical properties significantly improved when the content reached 4 parts. Sim *et al.* studied the addition of aluminum oxide and zinc oxide to the rubber, which greatly improved the thermal stability and thermal conductivity of SR [10]. However, the crystal surface of metal oxides contains a limited number of active sites, resulting in low antioxidant efficiency. Therefore, a significant dosage is required to realize the heat resistance, which will inevitably pose a challenge on achieving a desirable mechanical property. In this case, the development of novel rubber antioxidants with low dosage, simple and non-toxic synthesis, and effective antioxidant properties is of great importance and economic benefit for the sustainable growth of the rubber industry.

As discussed in the previous section, it is difficult to obtain satisfactory thermal aging-resistant composites by simple blending with a small amount of traditional metal oxides. Unlike metal oxides with low catalytic activity, metal-organic frameworks (MOFs)

* Corresponding authors.
E-mail addresses: longfeitan@mail.ipc.ac.cn (L. Tan), czh@cczu.edu.cn (Z. Chen), mengxw@mail.ipc.ac.cn (X. Meng).

https://doi.org/10.1016/j.cclet.2024.109669
1001-8417/

are considered as novel catalysts for various applications due to the superior electron channel provided by the organic molecular skeleton and the ultrafast transport of reactants, products, and electrolytes facilitated by the ordered porous structure [11,12]. Importantly, the topology and metal nodes of MOFs can be easily modified to optimize their catalytic performance. Considering the synthesis procedures, stability and the possibility for mass production MOFs, Co-MOF shows significant competitiveness in aspects involving its universal synthesis strategy and the flexibility in adjusting the yield according to practical demands [13]. Cobalt ions in Co-MOF can switch between the Co^{2+} and Co^{3+} states after absorbing and desorbing oxygen. Since metal ions in different oxidation states can scavenge free radicals by promoting electron transfer, Co-MOF can act as free radical scavenger [14,15]. Meanwhile, introducing other metals to create heterogeneous metal MOFs allows for the utilization of diverse active centers in constructing cascade reaction catalysts to achieve synergistic catalysis [16]. Due to the unique structure and flexible transition of valence states between Ce^{3+}/Ce^{4+} and the active site, doping cerium ions in Co-MOF succeed to improve the ability to scavenge free radicals [17,18]. Moreover, the ligand 2-methylimidazole of Co-MOF is composed of C–C and C–N bonds, which has a lower bond energy than Si-O-Si. Therefore, during thermal oxidation, the structure of Co-MOF collapses and forms smaller crystals. This exposes more metal ions on the crystal surface to capture free radicals and terminate free radical degradation of the polymer chain. Nevertheless, the dispersion and compatibility issues between MOFs and polymers during the preparation process have yet to be fully resolved, which will lead to the decreased in the performance of SR [19,20].

The solution for mitigating nonuniform MOFs dispersion is to attach the MOFs to strengthening agents, the indispensable elements in rubber products to improve their mechanical properties and lower expenses. Silica is an ideal carrier for grafting antioxidants due to its good reinforcing effect, low cost and abundant surface Si-OH groups. Compared with traditional silica nanoparticles, dendritic mesoporous organosilica nanoparticles (DMONs) exhibit three-dimensional (3D) central radial nanochannels, greater pore permeability, and more open channels, making them useful as carrier materials for supporting catalysts in the field of catalysis. In addition, the introduction of organic O-Si-R-Si-O into the inorganic Si-O-Si skeleton brings about the biocompatibility and hydrophobicity, significantly expanding the range of applications compared with inorganic dendritic mesoporous silica nanoparticles (DMSNs) [21,22]. To our knowledge, there is a dearth of research on the synthesis of composite MOFs/organosilica nanoparticles with antioxidant properties for low-filler heat-resistant rubber.

Although thermal stability of the SR composites has been improved owing to the advancing research on antioxidants, the mechanical strength after the heat treatment remains a challenge and impede the durability and lifetime of the silicone composites. For example, Zhao *et al.* [23] found the initial degradation temperature of SR was delayed by 40 °C with 37.5 parts of nano-Fe_2O_3, but its mechanical properties were significantly reduced. Li *et al.* [24] found that after adding 40% cerium oxide, the thermal oxygen stability of rubber was improved, but the tensile strength decreased. Herein, with a novel antioxidant-anchored silica surface enhancement strategy, which helps to synergistically enhancing the thermal and mechanical properties of the SR composite, instead of ignoring or even sacrificing the mechanical strength while improving the thermal stability as usual. We prepared DMONs@CeCo-MOF (DCCM) *via* a solution-assisted method by growing CeCo-MOF *in-situ* in DMONs, and SR composites were prepared with the general mixing and curing method shown in Scheme 1. Loading MOFs in dendritic mesoporous organosilica nanoparticles effectively addresses the issue of nonuniform dispersion between MOFs and the rubber matrix. The disulfide bonds

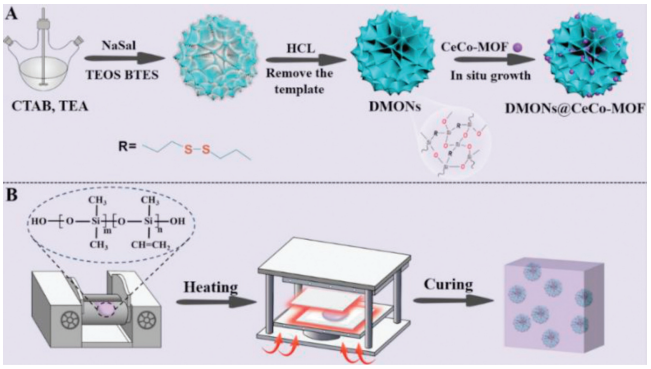

Scheme 1. Schematic diagram of the preparation of DCCM/SR composites.

in DMONs adsorb cerium and cobalt ions, which is essential to prepare CeCo-MOF and DMONs composites. As a result, the high oxygen catalytic efficiency and good dispersion bring about superb aging resistance at filler fractions as low as 0.5 phr. The successful synthesis of DCCM was demonstrated by transmission electron microscopy (TEM), X-ray photoelectron spectroscopy (XPS) and X-ray diffraction (XRD), and the effects of filler structure and antioxidants filler dispersion on thermal stability and mechanical properties of SR composites were studied systematically. We demonstrated that the strategy of organosilica@CeCo-MOF as antioxidant products showed significant potential in the "green rubber" sector.

The morphology and composition of all the samples were characterized by TEM and scanning electron microscopy (SEM). DMONs had a large open pore morphology with the size of about 200 nm (Fig. 1A). Compared to DMONs, nanoparticle accumulation (indicated by arrows in Fig. 1B) was found on the surface of DCCM, resulting in a relatively rough surface. CeCo-MOF generally grew in large pores and was extruded to the outer surface. Because of the environment in which nucleation growth occurred, the particle size was constrained. SEM (Fig. 1C) was further conducted to characterize DCCM. Small particle accumulations were observed on the surface of DCCM, and the initial open pores were reduced accordingly. This phenomenon was also observed in the TEM results. Energy dispersive X-ray (EDX) elemental mapping images (Fig. 1D) demonstrated even distribution of Si, Co and Ce elements in DCCM nanocomposites, indicating the coexistence of multiple elements. The average particle size of DCCM in an ethanol solution was measured using a laser particle size analyzer, and the results indicated an average size of approximately 300 nm (Fig. S1A in Supporting information). The zeta potential changes of the synthesized samples also demonstrated the successful preparation of DCCM nanocomposites (Fig. S1B in Supporting information). The measured potential of CeCo-MOF in water was positive (+22 mV), which was the same as that of Co-MOF aqueous solution. In contrast, the potential changed from negative charge of DMONs (−16 mV) to positive charge of DCCM (+2 mV), proving the successful growth of CeCo-MOF. The XRD patterns of the prepared precursor (Fig. S1C in Supporting information) agreed well with previous results [25], indicating that the addition of cerium ions did not impact the crystal structure of Co-MOF. In contrast to the crystalline framework of CeCo-MOF, the XRD pattern of DMONs showed amorphous state and did not show any obvious crystalline characteristic peaks. DCCM exhibited typical peaks that can be indexed to 011, 002, 112, 022, 013 and 222 diffractions of CeCo-MOF, although the intensity of the diffraction peaks was significantly reduced (Fig. 1E). Additionally, to confirm the successful construction of DCCM nanocomposites, various samples underwent X-ray photoelectron spectroscopy (Fig. 1F). Figs. S2A and B (Supporting information) showed that the peaks of O 1s and Si 2p appeared on

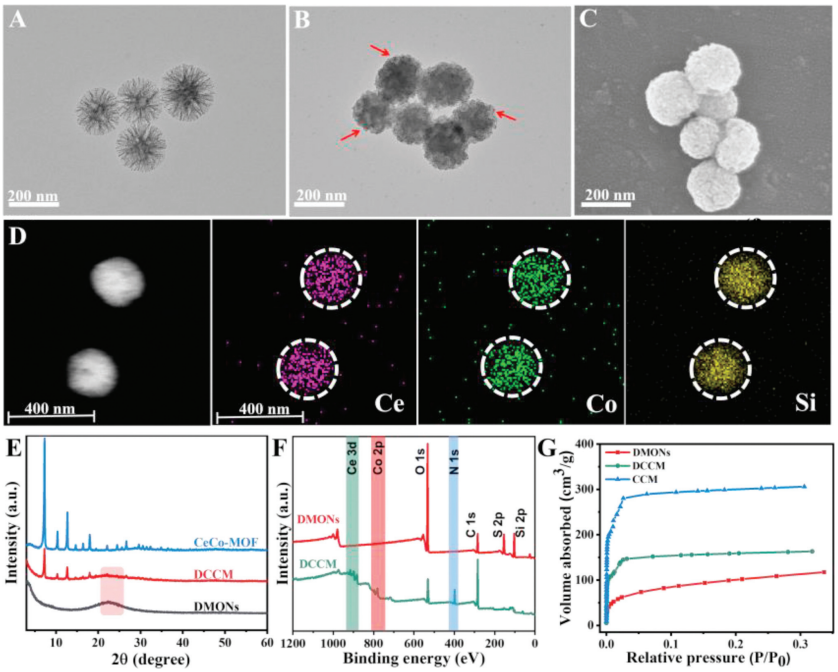

Fig. 1. (A, B) TEM images of DMONs and DCCM, respectively. (C) SEM images of DCCM. (D) Scanning transmission electron microscopy and element mapping (STEM) of DCCM. (E) XRD patterns of CeCo-MOF, DMONs and DCCM. (F) XPS spectra of DMONs and DCCM. (G) N_2 adsorption isotherm of various formulations.

the surface of DMONs, indicating that the basic composition of its skeleton structure is silica. The peak near 164 eV can be attributed to S 2p, which may originate from the disulfide bonds of DMONs. Subsequently, the main peak at 398.48 eV in the deconvoluted N 1s spectrum could be corresponded to N of the 2-methylimidazole ligand [26]. The Co 2p spectrum (Fig. S2E in Supporting information) was resolved into four intense main peaks (780.78, 782.61, 796.28 and 797.26 eV) and two weak satellite peaks (787.06 and 803.29 eV) [27]. it could be determined that the peaks of 782.61 and 797.26 eV represented Co^{3+}, and the peaks of 780.78 and 796.28 eV represented Co^{2+} [28,29]. As shown in Fig. S2F (Supporting information), the Ce 3d signal can be separated into eight peaks. Among them, the peaks of 903.78 and 885.28 eV corresponded to Ce^{3+}, whereas the other peaks were ascribed to Ce^{4+} [30,31]. We observed Co 2p, Ce 3d, and N 1s peaks emerging in DCCM compared with DMONs, confirming the successful loading of CeCo-MOF. In addition, to comprehend the impact of organosilica on the formation of DCCM, we prepared inorganic dendritic mesoporous silica nanoparticles (DMSNs) as a control. CeCo-MOF (Figs. S3A and B in Supporting information) had a rough surface, exhibited a rhombohedral dodecahedral morphology with an average grain size of about 500 nm. Figs. S3C and D (Supporting information) showed that CeCo-MOF nucleated and grew independently, with only a small fraction being loaded onto the surface of DMSNs. The presence of disulfide bonds in DMONs is deemed crucial for preparing CeCo-MOF and DMONs composites. Fig. 1G displayed the measurement results of N_2 adsorption isotherms for various samples. After the *in-situ* growth of CeCo-MOF, the specific surface area of DCCM was up to 527.2 m^2/g, which was higher compared with specific surface area of DMONs (367.5 m^2/g). However, the specific surface area of CeCo-MOF was approximately 967 m^2/g, the modest increased in the specific surface area of DCCM may be attributed to the comparatively low weight ratio of CeCo-MOF inside DMONs. The pore diameter and pore volume decreased after CCM modification (Fig. S1D in Supporting information), indicating the CCM partially occupied the mesopores of DMONs. Moreover, it can be seen from Figs. S1E and F (Supporting information) that the residue of DCCM at 700 °C in air was SiO_2, and the actual residue was 50.1%. The weights of cerium ions and cobalt ions in DCCM are 16.86% and 7.49% (Fig. S4 in Supporting information), respectively. Therefore, all results indicated the successful construction of DCCM nanocomposites.

The homogeneous dispersion of fillers within the polymer matrix results in exceptional overall properties of composite materials. Fig. S5 (Supporting information) displayed the SEM images of antioxidants in DCCM/SR composites with various dosing systems. Because of the insufficient interfacial bonding force between CeCo-MOF (CCM) and rubber, incompatible defects such as cavities and faults arise within the internal cross-linked network. On the contrary, the results showed that as the content of DCCM increased (Figs. S5A–C), no obvious large-area aggregates appeared. The interface between DCCM and SR was in a fuzzy state, showing excellent compatibility with the rubber molecular chain. This may be attributed to the similar molecular structure to silicone rubber, and the unique 3D network structure of DMONs exposes more active sites, resulting in an increase in the amount of bound rubber and enhanced interfacial interaction. The mechanical properties of DCCM/SR composites improved to a certain extent with an increase in the DCCM content (Fig. S6 in Supporting information). However, the content of DCCM should not exceed 2 parts for the overall high-level mechanical properties of DCCM/SR composites.

In order to observe the effect of antioxidant DCCM on the long-term aging resistance of rubber matrix, as shown in Fig. 2A, attenuated total reflectance-Fourier transform infrared spectroscopy (ATR-FTIR) was utilized to examine the alterations in the chemical structure of SR and DCCM/SR composites following diverse thermal oxidation durations. Thermal oxygen aging first destroys the side methyl group of DCCM/SR1 and gradually decomposes some small molecular substances. The Si-CH_3 absorption peak at 785 cm^{-1} and the Si-O-Si absorption peak at 1007 cm^{-1} was decreased and the peak area decreased gradually with the increase of aging time. The decrease in intensity at 785 cm^{-1} further suggests that the molecular side chain was broken or/and the methyl group was oxidized. The peak at 1007 cm^{-1} also gradually decreased with increasing aging time, indicating that the main chain of the DCCM/SR1 molecule was attacked. The crosslinking reaction and

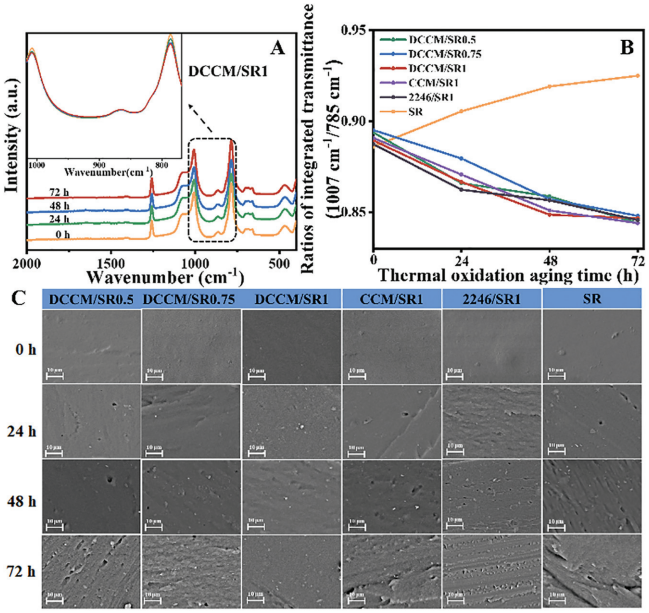

Fig. 2. (A) ATR-FTIR spectra of DCCM/SR1 during aging at 250 °C for different hours. (B) Ratios of integrated intensity of the transmittance measured and calculated for all SR composites. (C) SEM photos of all samples surface at different thermal oxidation aging time. Scale bar: 10 μm.

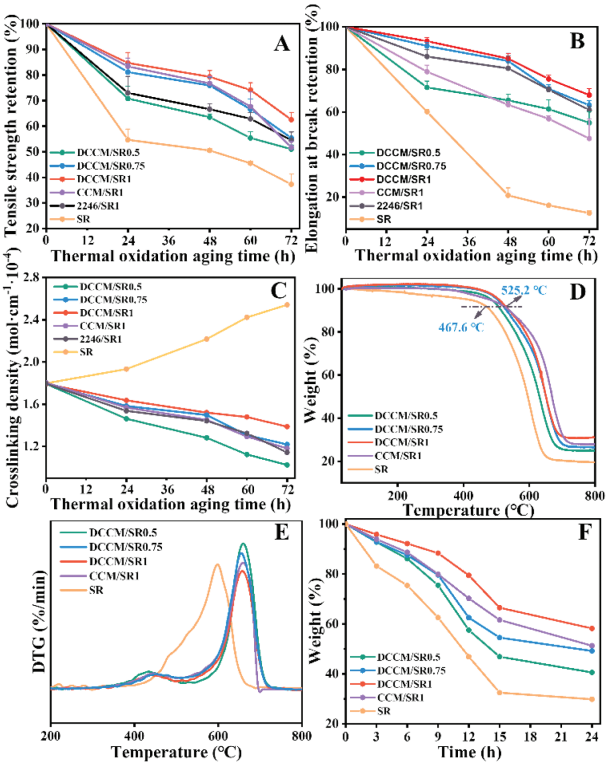

Fig. 3. Retention of (A) tensile strength and (B) elongation at break of DCCM/SR composites at different thermal oxidation aging time. (C) Crosslink density trends of SR composites at different thermal oxidation aging time. (D) TGA curves of all SR composites before aging. (E) DTG curves of all SR composites before aging. (F) Isothermal weight loss curves of all SR composites within 24 h. Data are presented as mean ± SD ($n = 3$).

degradation reaction occurred simultaneously during the thermal degradation process of SR, and the dominant reactions varied at different degradation stages [32]. To get additional helpful information on chemical structure changes, the ratio of the transmittance integrated intensity at 1007 cm^{-1} to that around 785 cm^{-1} was computed as a function of aging time, as shown in Fig. 2B. The ratio illustrated that the DCCM/SR composites progressively decreased with aging process, implying an inhibition of side chain oxidation reaction. The primary reaction at this stage involved the rearrangement and degradation of the backbone, which occurred at high temperatures. It is worth noting that the proportion of SR exhibited a steady increase over the course of the experiment, suggesting that the oxidation and cleavage of SR side groups predominantly transpired during the aging reaction competition process. As the duration of aging increases, gradual oxidation results in a reduction in cross-linking of molecular chains in the side chains. Simultaneously, the main chain is vulnerable to rearrangement reactions, generating new Si-O bonds and broken molecules, ultimately affecting the increased ratio.

The aging damage of heat and oxygen on the surface of all samples were observed by scanning electron microscopy. Fig. 2C showed DCCM/SR composites had no obvious damage in the early stages of aging, with the surface conditions being flat and smooth. With increased of aging time, cracks and cavities appeared on the surface of SR composites under the continuous attack of heat and oxygen. It was worth noting that the surfaces of the 2246/SR1, CCM/SR1, and SR samples exhibited severe damage following 72 h of thermal oxygen aging, whereas the DCCM/SR1 sample showed better thermal oxygen aging resistance compared to the aforementioned samples. Throughout the entire process of thermal-oxidative aging, DCCM demonstrated highly effective and enduring protective performance by promptly responding and efficiently scavenging the free radicals produced.

Reactive radicals resulting from the thermal and oxidative degradation of composites may result in decreased mechanical properties and changed cross-linking levels. However, the inclusion of DCCM effectively hindered the SR matrix oxidation. It is essential to assess the impact of DCCM on the mechanical characteristics of SR during thermos-oxidative aging. After 72 h of aging, the blank SR experienced a drop in its tensile strength (TS) retention and elongation at break (EAB) retention to approximately 37.3% and 12.5%, respectively (Figs. 3A and B). The incorporation of just 0.5 phr DCCM resulted in a significant improvement in mechanical properties after aging, with an increase in the retention of tensile strength and elongation at break to 51% and 54.9%, respectively. With DCCM/SR1, the final retention of EAB was as high as 68%, which was about 55% higher than SR. The mechanical properties were greatly enhanced in comparison to 2246 antioxidant after aging, indicating that DCCM is a more effective antioxidant than 2246 antioxidant. Moreover, gradually incorporating DCCM resulted in sustained improvements in the retention of EAB after aging without loss of TS of the composites. The crosslinking density of the SR sample increased during the thermal oxygen aging process as shown in Fig. 3C, suggesting that the crosslinking reaction was dominant and in the crosslinked structure was also changed. Conversely, DCCM/SR composites displayed decreased crosslinking density with time. The thermal oxidation reaction of DCCM/SR had undergone a significant change, effectively blocking the crosslinking reaction in the side chain. As a result, the thermal degradation process was promoted or accelerated by backbone rearrangements that occurred at higher temperatures.

Thermogravimetry analysis (TGA) can be used to study the thermal decomposition of substances. Fig. 3D showed the thermogravimetry analysis (TG) curve of DCCM/SR composites under nitrogen condition. Considering the composition of various composites, the initial weight loss is likely caused by some low molecular material. Based on the data, the temperature with a weight loss of 10 wt% was chosen as the initial degradation temperature (T_{10}) of SR. T_{10} was observed to increase by approximately 58 °C from

467.6 °C of SR to 525.2 °C of DCCM/SR1. It was worth mentioning that the T_{10} of all DCCM/SR composites was higher than SR due to the addition of DCCM. It was also identified that the maximum rate of mass loss temperature was also delayed by 59.1 °C from 601.7 °C (SR) to 660.8 °C (DCCM/SR1). Polysiloxanes are recognized for unzipping degradation in the presence of impurities containing hydroxyl, resulting in volatile cyclic products at high temperatures [33,34]. As demonstrated in Fig. 3E, the obvious weight loss peak appears at 600–900 °C. During this stage, rearrangement of Si-O bonds in the polysiloxane system leads to the eventual formation of a cyclic structure molecular chain [35]. The DCCM antioxidants prevented oxidation of side chains and slowed the process of thermal degradation in the overall matrix.

Compared with TGA, isothermal weight loss testing provided a more intuitive evaluation of the thermal stability of SR composites. Fig. 3F showed the spectra of mass loss of SR, DCCM/SR composites and CCM/SR composites under different aging times. The side chain of SR underwent an oxidative cleavage reaction under continuous exposure to high temperature and oxygen. As a result, SR experienced a 23% loss in mass after 6 h, while DCCM/SR1 only experienced a 5% reduction in mass. The incorporation of DCCM into the siloxane system prevented side chain breakage and significantly enhanced the heat resistance of DCCM/SR composites. After 24 h of aging, the mass retention rate of DCCM/SR1 remained at 64%, exceeding that of SR (29%) by 35%. If the ideal process of nearly complete degradation of the side group of the blank SR is pursued, the resulting remaining state would be silica. Based on the analysis of derivative thermogravimetry (DTG) results, the degradation of pure SR at 350 °C was primarily attributed to the oxidative cleavage of the side chains.

Thermal oxidation of SR follows the free radical oxidation mechanism similar to the oxidation of polysiloxane [36]. The interaction between free radicals and DCCM is a potential explanation for the antioxidant function of DCCM in SR. The electron spin resonance (ESR) spin trapping analysis was conducted on the samples to assess the potential reaction mechanism of DCCM antioxidants with free radicals. SR generated a series of free radicals during thermal oxygen aging. One of these is the hydroxyl radical, which is commonly chosen to evaluate the ability to scavenge free radicals. Hydroxyl radical reportedly has a brief lifespan and reacts quickly. The spin-trap 5,5-dimethyl-1-pyrroline *N*-oxide (DMPO) is frequently utilized to react with hydroxyl radical in the formation of stable free radical adducts (DMPO–OH), which are more easily detectable by ESR. The ESR spectrum displaying the quartet signal of DMPO–OH with an intensity ratio of 1:2:2:1 was featured in Fig. 4A, representing the DMPO–OH adduct. However, the addition of DCCM resulted in a significant decreased in signal intensity for the DMPO–OH adduct, indicating that DCCM is a potential scavenger of hydroxyl radicals. Since CO_2 is a typical gas degradation byproduct generated during thermal oxidation of SR composites, evaluation of the aging of the material can also be achieved through the CO_2 peak area in the infrared spectrum. The high CO_2 generation rate of SR in Fig. 4B suggests the worst thermal stability, whereas the DCCM/SR1 sample reduced CO_2 production by almost 50%. The physical properties and morphology of aged SR were studied by characterizing the main elements (C, O and Si) on the surface of SR before and after aging. According to the peak area of the surface element C, O and Si in Fig. S7 (Supporting information), the percentage of these element can be calculated as shown in Table S2 (Supporting information). The proportion of C element reduces, while the proportion of element O and Si increase. It can be concluded that the chemical reaction of silicone thermal oxidative degradation is mainly the pendant group oxidative cross-linking reaction [37]. The results indicate that DCCM has enhanced radical scavenging activity and can efficiently hinder the crosslinking of rubber molecular chains under thermal-oxidative

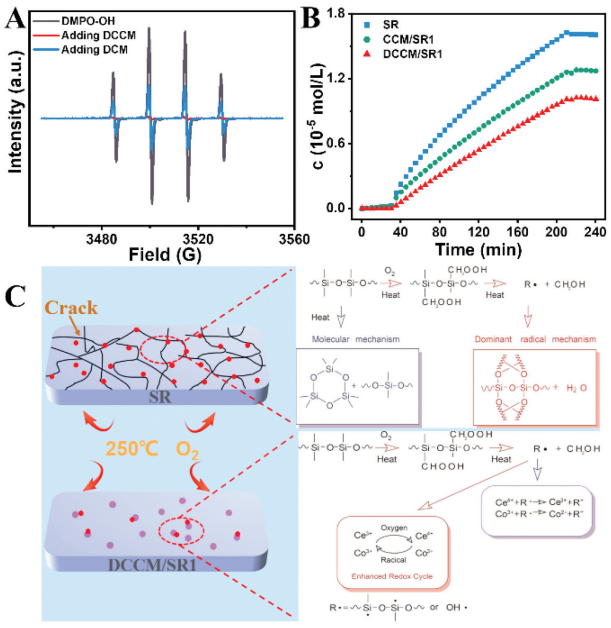

Fig. 4. (A) Typical ESR DMPO–OH signals obtained after adding different materials. (B) Generation of CO_2 of unaged SR composites for the *in-situ* test at 100 °C. (C) Possible mechanism of DCCM on improving the thermal-oxidative aging properties of SR.

aging conditions. Based on the above analyses, the possible mechanism of DCCM for SR was proposed as shown in Fig. 4C that, under continuous exposure to thermal and oxygen, SR can remarkedly increase the level amounts of peroxyl radicals and accelerate the crosslinking and degradation of side chain. For DCCM/SR composites, we showed that DCCM effectively eliminated free radicals generated by molecular chain breakage and inhibited the breakage of side chain Si-C bonds. This eventually led to thermal oxygen reactions by degrading the main chain. On the one hand, DMONs can physically or chemically combine with SR macromolecules to create an adsorption layer of SR molecules on the silica surface, enhancing the compatibility of DCCM within polymers [38]. On the other hand, Ce^{4+} and Co^{3+} could generate stable compounds by complexing with free radicals and transforming into Ce^{3+} and Co^{2+}. Notably, Ce^{3+} and Co^{2+} were re-oxidized to Ce^{4+} and Co^{3+} by contacted with external oxygen to ensure that the radicals were continuously quenched. Therefore, it could be concluded that DCCM positively affected the thermo-oxidative stability of SR.

Due to concerns pertaining to volatilization, migration, and extractability of low molecular weight rubber antioxidants, the dosage should not surpass the solubility threshold within the rubber matrix to avert blooming and contamination of the rubber surface. Moreover, in situations of severe load conditions, antioxidants move to the surface of the rubber items at an increased pace, leading to the unavoidable occurrence of blooming. Loading rubber additives on the surface of nanofillers has been effectively reduce the migration of rubber additives. Fig. S8 (Supporting information) illustrated an observation of numerous precipitates that emerged on the previously even surface of the CCM/SR1 composites within 3 days. The DMONs restricted the evasion and movement of antioxidants, resulting in minimal precipitation on the surface of DCCM/SR1 composites sample. The result was further confirmed by the energy dispersive spectrometer (EDS) spectrum of the "blooming" material in the SEM photo. DCCM can be uniformly distributed within the rubber matrix and efficiently intertwined with the rubber molecular chains. At the same time, improving the volatility and migration resistance of antioxidants in the ma-

trix, whereas incorporating the same number of free antioxidants exacerbated blooming.

In summary, we have employed a facile and low-cost solution-assisted method to synthesize a novel antioxidant DCCM by growing CeCo-MOF *in situ* on the surface of DMONs. For the first time, DCCM was mixed with SR to serve as rubber antioxidant *via* the most common two-roll milling process. DCCM functioned as an efficient antioxidant and a compatibilizer of the rubber-filler interface, exhibiting outstanding long-term thermal oxidation protection, physical and mechanical properties, and notably resisting migration of small molecule reagents. Besides, by incorporating cerium ions, DCCM displayed a more potent free radical trapping capacity. The comprehensive proposal for the cross-linking and degradation mechanism of DCCM/SR composite materials in a thermal oxygen environment was achieved through analyzing the alterations in material structure and properties. The synthesis of MOF consumes many solvents, although these solvents are eco-friendly (such as water, ethanol). Recovering and recycling the solvent used in the production of MOFs can help reduce the production cost of MOFs and minimize resource waste. However, it is a challenge for MOFs materials to achieve a technological leap from laboratory gram-level synthesis to mass production under current processing conditions. This work offers novel perspectives on the creation of polymers with low amounts of antioxidant and excellent aging resistance.

Declaration of competing interest

The authors declare that they have no known competing financial interests or personal relationships that could have appeared to influence the work reported in this paper.

Acknowledgment

The authors acknowledge financial support from the Beijing Natural Science Foundation (No. JQ23035).

Supplementary materials

Supplementary material associated with this article can be found, in the online version, at doi:10.1016/j.cclet.2024.109669.

References

[1] A. Charlesby, Nature 173 (1954) 679–680.
[2] S.W. Wu, P.J. Weng, Z.H. Tang, B.C. Guo, ACS Sustain. Chem. Eng. 4 (2016) 247–254.
[3] Y.K. Zou, J.W. He, Z.H. Tang, L.X. Zhu, F. Liu, Compos. Sci. Technol. 188 (2020) 107984.
[4] A. Karekar, K. Owald, K. Reincke, B. Langer, Macromolecules 53 (2020) 11166–11177.
[5] S.W. Wu, M. Qiu, B.C. Guo, L.Q. Zhang, Y. Lvov, ACS Sustain. Chem. Eng. 5 (2017) 1775–1783.
[6] H. Parvatareddy, J.Z. Wang, D.A. Dillard, T.C. Ward, Compos. Sci. Technol. 53 (1995) 399–409.
[7] Y.K. Sun, J.Z. Huang, J.W. He, et al., Polym. Degrad. Stab. 185 (2021) 109428.
[8] J.D. Qiu, X.J. Lai, H.Q. Li, X.R. Zeng, Z.P. Zhang, Polymers 10 (2018) 15.
[9] L. Wu, Y. Zhang, E-Polymers 19 (2019) 257–267.
[10] L.C. Sim, S.R. Ramanan, H. Ismail, K.N. Seetharamu, T.J. Goh, Thermochim. Acta 430 (2005) 155–165.
[11] H. Furukawa, K.E. Cordova, M. O'Keeffe, O.M. Yaghi, Science 341 (2013) 1230444.
[12] Y.T. Qin, Y. Wan, J. Guo, M.T. Zhao, Chin. Chem. Lett. 33 (2022) 693–702.
[13] R. Wu, X. Qian, X. Rui, et al., Small 10 (2014) 1932–1938.
[14] G. Saracco, S. Vankova, C. Pagliano, B. Bonelli, E. Garrone, Phys. Chem. Chem. Phys. 16 (2014) 6139–6145.
[15] Q.H. Gao, J. Li, Y.C. He, et al., Polym. Degrad. Stab. 190 (2021) 109622.
[16] H.N. Yu, H.C. Xia, J.N. Zhang, et al., Chin. Chem. Lett. 29 (2018) 834–836.
[17] C.Y. Dong, Y. Zhou, N. Ta, et al., Chin. J. Catal. 42 (2021) 2234–2241.
[18] Y.Q. Sun, Y. Guan, X.C. Wu, et al., Nanoscale 13 (2021) 3227–3236.
[19] S.Y. Rong, P.C. Su, S.Z. Chen, M.M. Jia, W.B. Li, Chin. Chem. Lett. 33 (2022) 2134–2138.
[20] Z. Wang, D. Wang, S. Zhang, L. Hu, J. Jin, Adv. Mater. 28 (2016) 3399–3405.
[21] Z. Guo, H. He, Y. Zhang, et al., Chen, Adv. Mater. 33 (2021) 2004225.
[22] B. Liu, L. Feng, Y. Bian, et al., Adv. Healthc. Mater. 11 (2022) e2200665.
[23] B. Zhao, Q.L. Wang, L. Jin, Sci. Eng. Compos. Mater. 20 (2013) 331–335.
[24] L. Mei, Z.X. Shi, Z.G. Liu, et al., J. Rare. Earth. 25 (2007) 138–141.
[25] Q. Shi, Z. Chen, Z. Song, J. Li, J. Dong, Angew. Chem. 50 (2011) 672–675.
[26] G. Yu, J. Sun, F. Muhammad, P. Wang, G. Zhu, RSC Adv. 4 (2014) 38804–38811.
[27] S. Ahmed, J. Shim, H.J. Sun, G. Park, Phys. Status. Solidi. 217 (2020) 1900969.
[28] S. Xie, Q. Qin, H. Liu, et al., ACS Appl. Mater. Inter. 12 (2020) 48476–48485.
[29] H. Dai, W. Zhou, W. Wang, Chem. Eng. J. 417 (2021) 127921.
[30] G. Pantaleo, V.L. Parola, F. Deganello, et al., Appl. Catal. B 189 (2016) 233–241.
[31] J. Chen, W. Shi, J. Li, Catal. Today 175 (2011) 216–222.
[32] G. Camino, S.M. Lomakin, M. Lageard, Polymer 43 (2002) 2011–2015.
[33] E.W. Jia, S.J. Zhao, Y.G. Shangguan, Q. Zheng, Compos. Sci. Technol. 184 (2019) 107846.
[34] Y. Han, J. Zhang, L. Shi, et al., Polym. Degrad. Stab. 93 (2008) 242–251.
[35] X.W. Zhao, C.G. Zang, Y.Q. Wen, Q.J. Jiao, J. Appl. Polym. Sci. 132 (2015) 42582.
[36] A.N. Zheng, Y.K. Huang, Y. You, et al., Polym. Degrad. Stab. 158 (2018) 168–175.
[37] J. Wu, J.Y. Dong, Y.S. Wang, K.G. Bipin, Polym. Degrad. Stab. 35 (2017) 43–53.
[38] J.W. Brinke, S.C. Debnath, L. Reuvekamp, J.W.M. Noordermeer, Compos. Sci. Technol. 63 (2003) 1165–1174.